

Angular and planar transport properties of antiferromagnetic V_5S_8

Xiao-Kai Wu(吴晓凯), Bin Wang(王彬), De-Tong Wu(吴德桐), Bo-Wen Chen(陈博文), Meng-Juan Mi(弭孟娟), Yi-Lin Wang(王以林), and Bing Shen(沈冰)

Citation: Chin. Phys. B, 2024, 33 (**2**): 027503. DOI: 10.1088/1674-1056/ad15f9
Journal homepage: http://cpb.iphy.ac.cn; http://iopscience.iop.org/cpb

What follows is a list of articles you may be interested in

A spin-based magnetic scanning microscope for *in-situ* strain tuning of soft matter

Zhe Ding(丁哲), Yumeng Sun(孙豫蒙), Mengqi Wang(王孟祺), Pei Yu(余佩), Ningchong Zheng(郑宁冲), Yipeng Zang(臧一鹏), Pengfei Wang(王鹏飞), Ya Wang(王亚), Yuefeng Nie(聂越峰), Fazhan Shi(石发展), and Jiangfeng Du(杜江峰)

Chin. Phys. B, 2023, 32 (**5**): 057504. DOI: 10.1088/1674-1056/acbaee

Dynamical signatures of the one-dimensional deconfined quantum critical point

Ning Xi(西宁) and Rong Yu(俞榕)

Chin. Phys. B, 2022, 31 (**5**): 057501. DOI: 10.1088/1674-1056/ac5987

Ionic liquid gating control of planar Hall effect in $Ni_{80}Fe_{20}/HfO_2$ heterostructures

Yang-Ping Wang(汪样平), Fu-Fu Liu(刘福福), Cai Zhou(周偲), Chang-Jun Jiang(蒋长军)

Chin. Phys. B, 2020, 29 (**7**): 077507. DOI: 10.1088/1674-1056/ab8da9

Magnetic properties and magnetocaloric effects in $Er_{1-x}Gd_xCoAl$ intermetallic compounds

Gao Xin-Qiang (高新强), Mo Zhao-Jun (莫兆军), Shen Jun (沈俊), Li Ke (李珂), Dai Wei (戴巍), Wu Jian-Feng (吴剑峰), Tang Cheng-Chun (唐成春)

Chin. Phys. B, 2015, 24 (**9**): 097502. DOI: 10.1088/1674-1056/24/9/097502

Magnetization reversal process in Fe/Si (001) single-crystalline film investigated by planar Hall effect

Ye Jun (叶军), He Wei (何为), Hu Bo (胡泊), Tang Jin (汤进), Zhang Yong-Sheng (张永圣), Zhang Xiang-Qun (张向群), Chen Zi-Yu (陈子瑜), Cheng Zhao-Hua (成昭华)

Chin. Phys. B, 2015, 24 (**2**): 027505. DOI: 10.1088/1674-1056/24/2/027505

RAPID COMMUNICATION

Angular and planar transport properties of antiferromagnetic V_5S_8

Xiao-Kai Wu(吴晓凯)[1], Bin Wang(王彬)[1], De-Tong Wu(吴德桐)[1], Bo-Wen Chen(陈博文)[1], Meng-Juan Mi(弭孟娟)[2], Yi-Lin Wang(王以林)[2], and Bing Shen(沈冰)[1,†]

[1] *Center for Neutron Science and Technology and School of Physics, Guangdong Provincial Key Laboratory of Magnetoelectric Physics and Devices, and Key Laboratory of Optoelectronic Materials and Technologies, Sun Yat-Sen University, Guangzhou* 510275, *China*

[2] *School of Integrated Circuits, Shandong Technology Center of Nanodevices and Integration, State Key Laboratory of Crystal Materials, Shandong University, Jinan* 250100, *China*

(Received 16 November 2023; revised manuscript received 12 December 2023; accepted manuscript online 15 December 2023)

Systemically angular and planar transport investigations are performed in layered antiferromagnetic (AF) V_5S_8. In this AF system, obvious anomalous Hall effect (AHE) is observed with a large Hall angle of 0.1 compared to that in ferromagnetic (FM) system. It can persist to the temperatures above AF transition and exhibit strong angular field dependence. The phase diagram reveals various magnetic states by rotating the applied field. By analyzing the anisotropic transport behavior, magnon contributions are revealed and exhibit obvious angular dependence with a spin-flop vanishing line. The observed prominent planar Hall effect and anisotropic magnetoresisitivity exhibit two-fold systematical angular dependent oscillations. These behaviors are attributed to the scattering from spin–orbital coupling instead of nontrivial topological origin. Our results reveal anisotropic interactions of magnetism and electron in V_5S_8, suggesting potential opportunities for the AF spintronic sensor and devices.

Keywords: antiferromagnetism, planar Hall effect, magnetic and topological properties

PACS: 75.20.En **DOI:** 10.1088/1674-1056/ad15f9

1. Introduction

Antiferromagnet (AFM) materials have been considered as promising candidates for next-generation spintronic devices due to the scalability, robustness and ultrafast spin dynamics.[1] In an AF system, considering the special symmetry, the complicated magnetic correlations interacted with electron bands or phonon will host various exotic states driving novel transport properties as in ferromagnetic (AF) materials.[2] For example, recent studies revealed large anomalous Hall effect in noncolinear or topological AF systems such as Mn_3Sn,[2] $CoNb_3S_6$,[3] or GdPtBi.[4] Spin-polarized current or magnetic spin Hall effect have been theoretically predicted and experimentally observed in Mn_3Sn[5] and Mn_3Ir.[6] With further consideration of the spin-symmetry, altermagnetic (AM) materials are identified with collinear AF order and exhibit unconventional spin-polarization order, providing new punch line for magnetism and spintronics.[7] Exploring the AF (or AM) magnetism in a two-dimensional (2D) or quasi-2D system will bring the dimension limitation which arouses types of novel magnetic or electronic states.[8,9] Such as in AF topological $MnBi_2Te_4$, the observed Chern state or axion state can drive quantized Hall conductance.[10]

For layered magnetic V-based chalcogenides (V_mS_n), tunable structural phases and magnetic properties via stoichiometric variations will bring a good platform to investigate interplay of magnetism and topology.[11,12] Bulk 2D VS_2 exhibits ferromagnetism and metallic behavior.[13] The doped or intercalated magnetic impurities with unfilled 3d orbitals act as the scattering centers leading to the appearance of Kondo effect due to the exchange interactions between localized magnetic moments of the impurities and conduction electrons.[14–16] The large vacancies of sulfur would make system evolve to another $1T^1$-phase V_5S_8 with a fraction of the vanadium atoms inserted within the van der Waals gap between VS_2 layers (shown in inset of Fig. 1(b)). In bulk V_5S_8, the AF state dominates the system; while with decreasing thickness, the AF state will evolve to a spin-glass-like state and eventually to a weak ferromagnetic state.[17–22] The interaction of spin lattice and electron would host the possible nonzero Berry curvature or exotic surface states.[23,24] The tunable magnetic anisotropy and correlations make V_5S_8 a candidate for magnetic sensor which needs to investigate anisotropic magnetoresistivity (AMR) signal carefully for manipulating the spins in the AF system. On the other hand, recent study on VS_2–VS superlattice revealed an unconventional planar Hall effect that persisted to 380 K.[25] This observation enlightens us to explore exotic properties in the similar compound such as V_5S_8, a natural VS_2–V–VS_2 superlattice. In this paper, we investigate angular and planar transport properties of V_5S_8. Anisotropic AHE in a flopped state is identified with large Hall angle Θ up to 0.1. The phase diagram reveals a spin-flop vanishing line by rotating the applied field distinguishing the magneto-transport behaviors due to different magnon contributions. The prominent planar Hall effect (PHE) and

[†]Corresponding author. E-mail: shenbing@mail.sysu.edu.cn

© 2024 Chinese Physical Society and IOP Publishing Ltd

anisotropic mganetoresistivity (AMR) are observed. By analyzing the plots of scaled PHE and AMR curves, the prominent AMR signal is attributed to the orbital effect instead of the nontrivial topological origin, but still promising for AF sensor.

2. Experimental details

Single crystals of V_5S_8 were grown by the chemical vapor transport method using the pre-prepared V_5S_8 powder as precursors and I_2 as the transport agent. The mixture of V_5S_8 and I_2 were first heated at 500 °C (cold end) and 600 °C (hot end) in a two-zone furnace within five hours respectively and then kept for one week. Large plates of single crystals were harvested with a typical size of 2×2 mm^2. The crystal structure and elemental composition were checked by x-ray diffraction (XRD) measurements and energy-dispersive x-ray spectroscopy (EDS), respectively. Figure 1(a) shows the (00l) peaks for our single crystals, indicating the good crystalline of our samples. The selected crystal was shaped into a rectangle for the transport measurements as shown in Fig. 1(b). Six contacts were made by gold deposition to ensure a brilliant conductivity and the current was applied along the a axis of the crystal. Electrical transport measurements were performed in a physical properties measurement system (PPMS Dynacool, Quantum Design). Magnetization measurements were performed in the vibrating sample magnetometer (VSM) module of the PPMS.

3. Results and discussion

3.1. Short-range magnetism and anomalous Hall effect

The temperature dependent resistivity $\rho_{xx}(T)$ exhibits a metallic behavior as shown in Fig. 1(c) and an anomaly emerges around $T_{\rm AF} = 30$ K associated with the peak in temperature dependent susceptibility $\chi(T)$ due to the AF transition.[19,26–28] With increasing temperature, the long-range (LR) AF orders vanish. A region dominated by short-range (SR) magnetic orders from $T_{\rm AF}$ to $T_\theta = 196$ K is identified with $\chi(T)$ deviating the Curie–Weiss law.[29] The SR origin from magnetic fluctuation or frustration is widely observed in a magnetic system and may strongly affect its electron structure and transport behavior. Here, the frustrated parameter for V_5S_8 is calculated by $f = T_\theta/T_{\rm AF}$,[29] yielding a value of 6.175 indicating an intermediate magnetic frustration.

To explore the transport behaviors related to the AF and SR magnetic orders, field dependent magneto-resistivity (MR defined as $MR = (\rho_x x(\mu_0 H) - \rho(0))/\rho(0) \times 100\%$) and Hall resistivity $\rho_{xy}(\mu_0 H)$ are investigated at various temperatures as shown in Fig. 2(a). In the AF state (below $T_{\rm AF}$), nonlinear field dependent Hall effect and nonmonotonous field dependent MR are observed. At an intermediate field $\mu_0 H_{\rm SF}$, a clear step emerges in $\rho_{xy}(\mu_0 H)$ accompanied by a peak in MR, suggesting the occurrence of a spin-flop transition instead of possible breakdown of SDW or CDW transition consisted with previous work.[19,27] For a magnetic system, the Hall resistivity can be described as[30]

$$\rho_{xy} = \rho_{xy}^{\rm N} + \rho_{xy}^{\rm A} = R_{\rm N} B + R_{\rm A} M, \tag{1}$$

where R_0 and $R_{\rm A}$ are the ordinary and anomalous Hall coefficients, and M is the magnetization. The separated $\rho_{xy}^{\rm A}$ at various temperatures are shown in Fig. 2(c). In AF ground state, the $\rho_{xy}^{\rm A}$ keeps a small value while it increases sharply with a large Hall angle $\Theta = 0.15$ compared to that in FM system after the spin-flop transition. For an AF system, it is usually surprising to host obvious AHE reminiscent with the recently observed prominent AHE in AF topological materials with large Berry curvature or chiral magnetic materials with non-vanishing magnetization.[31–33] For V_5S_8, the $V_{\rm I}$ site is located in the layer where the vanadium vacancies are ordered (vacant layer), while $V_{\rm II}$ and $V_{\rm III}$ sites are in the layer without vanadium vacancies (full layer). Only the former contributes magnetism to the system. This conlinear AF ground state exhibits vanishing net magnetization, resulting in the negligible AHE and the positive MR. However, the spin-flopped state gives rise to an increased magnetization, leading to the extended AHE and negative MR due to the delocalization by the flopped moments from $V_{\rm I}$.

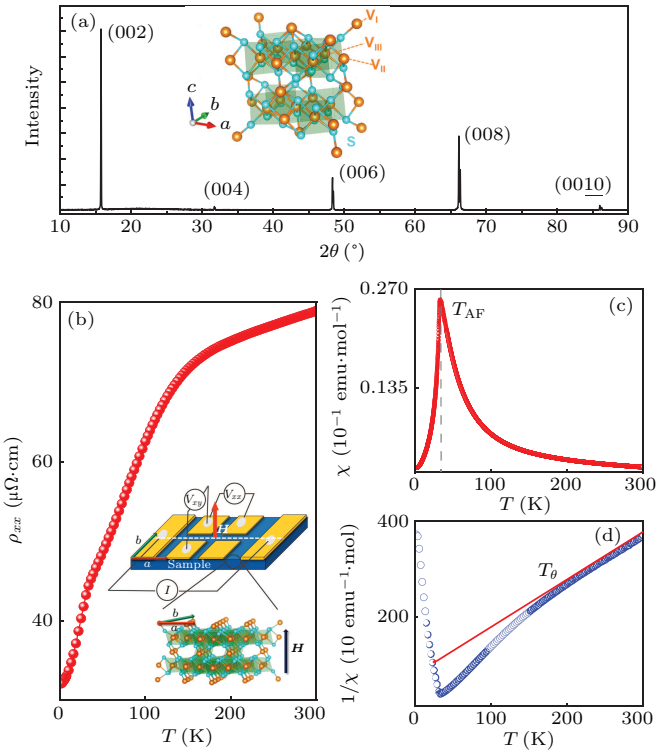


Fig. 1. (a) XRD pattern of single-crystalline V_5S_8 with the corresponding Miller indices (00l) in parentheses. Inset: Crystal structure of V_5S_8. (b) Temperature-dependent longitudinal resistivity of V_5S_8 with the current (I) along the axis. Inset: Schematic for our electronic measurement device of V_5S_8. (c) Temperature dependent magnetic susceptibility of V_5S_8 with $\mu_0 H = 1$ T. (d) The inverse of magnetic susceptibility fitted by the Curie–Weiss law.

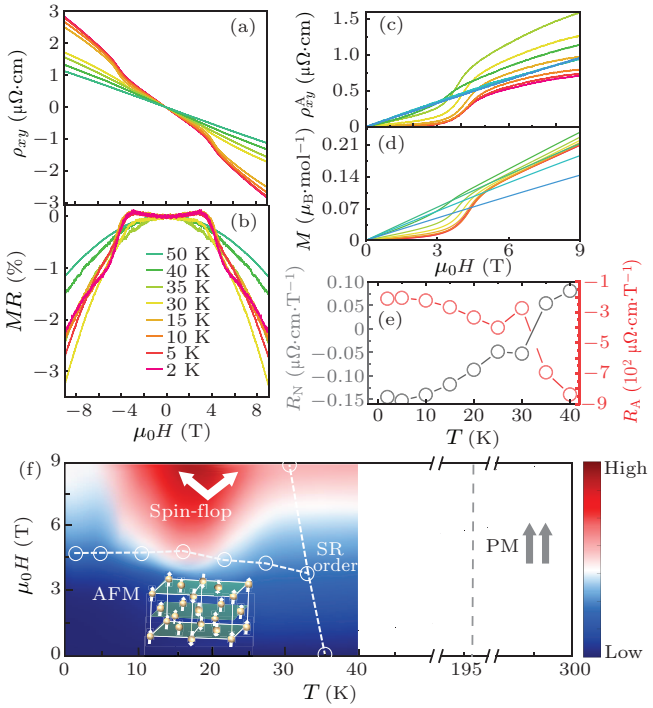


Fig. 2. Field dependent ρ_{xy} (a) and *MR* (b) at 2 K, 5 K, 10 K, 15 K, 30 K, 35 K, 40 K, 50 K with the applied magnetic field along the *c* axis of V_5S_8. (c) Anomalous Hall resistivity at different temperatures. (d) Field dependent magnetization curve at various temperatures. (e) The temperature dependent ordinary Hall coefficient R_N (black) and anomalous Hall coefficient R_A (red). (f) The phase diagram of V_5S_8 with $\mu_0 H \| c$ axis. The colors indicate anomalous Hall resistivity. Inset: Structure of V_5S_8 in the AFM phase.

With increasing the temperature above T_{AF}, LR AF order vanishes and the SR magnetic order dominates the system. The nonlinear field dependent Hall effect and and AHE (observed in temperature dependent R_A shown in Fig. 2(e)) can still persist in a narrow temperature region. The observed negative *MR* indicates that the SR magnetic order in this region exhibits FM correlations probably driven by spin fluctuations or frustrations. These behaviors are reminisced with the observed AHE and unconventional AHE above AF transition in topological $EuZn_2As_2$[34] and $EuCd_2As_2$.[35] These results suggest that in a magnetic system, the SR order can play an important role in shaping the electron structure and driving exotic transport properties even without LR orders. The phase diagram for V_5S_8 with the applied field along *c* axis is shown in Fig. 2(f). Due to the SR magnetic order, AHE emerges above T_{AF} and enhances with increasing the applied field. The negative *MR* can persist to even much higher temperature, indicating that this FM correlation exists in a wide temperature region.

3.2. Angular dependence of Hall effect and MR

To check the anisotropy in V_5S_8, angular transport measurements were performed with an applied field rotating in a plane perpendicular to the current direction (the *a* axis) as shown in the inset of Fig. 3(a). The nonlinear field dependent Hall effect and nonmonotonous field dependent *MR* systematically evolve and exhibit anisotropic behavior as shown in Figs. 3(a) and 3(b). The spin-flop transition at $\mu_0 H_{SF}$ becomes invisible gradually when rotating the applied field towards the *a* axis. To better check the angular dependence of the spin-flop transition, the differential ρ_{xy} curves ($d\rho_{xy}/d\mu_0 H$) at various angles are acquired and plotted as the function of out-of-plane field component $\mu_0 H_z = \mu_0 H \cos\theta$ as shown in Fig. 3(d). With tilting the applied field towards *ab* plane, H_{SF} almost does not shift and becomes invisible at $\theta_{SF} = 50°$ in consistent with the absence of the transition peak and positive response in *MR* curves. The phase diagram for V_5S_8 with the applied field rotating from the *c* to *a* axis is shown in Fig. 3(d). The spin-flop transition line roughly separates the system into two region: AFM region(I) and flopped magnetic region (II). In region I, the system keeps AFM structure with limited magnetization, leading to invisible AHE and the positive *MR*. In region II, the flopped spins with FM correlations due to the applied field dominate the system, leading to visible AHE and negative *MR* with the appearance of the obvious magnetization.

In the AF groud state, the magnetic moments of V_I in the (1 0 0) plane align ferromagnetically and are arranged like (up up down down) in the [1 0 0] direction, forming a staggered AF structure as shown in the inset of Fig. 2(f). The direction of the moments is tilted about 10.43° from the *c*-axis toward the *a*-axis.[28,36] Usually, the magnetic field affects the magnon spectrum by changing the Zeeman energy.[37] Thus, the magnon *MR* is determined by the component of the applied field along the magnetic easy axis. Our angular *MR* (especially for the flopped state) can not be simply scaled by a function of $\mu_0 H_z$. In V_5S_8, the magnetic easy axis is not strictly along the *c* axis of the crystal.[36] Thus the slight tilt of the magnetization away from the *z* axis by an in-plane field component would make the angular *MR* deviate from empirical scaling. In this case, the magnon *MR* is proportion to $M\mu_0 H(\cos\theta\cos\beta + \sin\theta\sin\beta)$, where M is the magnetization, θ is the angle between the applied field direction and *z* axis, and β is the angle between the magnetization direction and *z*.[38,39] With a small β, the *MR* can be expressed as[37]

$$\rho_{xx} = C_1 \mu_0 H \cos\theta + C_2 (\mu_0 H \sin\theta)^2, \tag{2}$$

where C_1 and C_2 are the coefficients independent of the applied field angle. The first part of this formula, following a linear field dependence, results from the magnetic moment, The second part, following a quadratic field dependence, can be well understood based on electron paramagnon scattering. C_1 and C_2 are acquired by fitting the above formula as shown in Fig. 3(f). With $\theta < \theta_{SF}$, the linear field dependent contribution mainly dominates the *MR* while the quadratic dependent contribution increases with tilting the applied field to the *ab* plane. At θ_{SF} where the spin-flop transition disappears, the linear field dependent contribution starts to decrease while the quadratic field dependent contribution becomes saturated. These behaviors reveal the magnetocrystalline anisotropy and anisotropic orbital scattering in V_5S_8.[40]

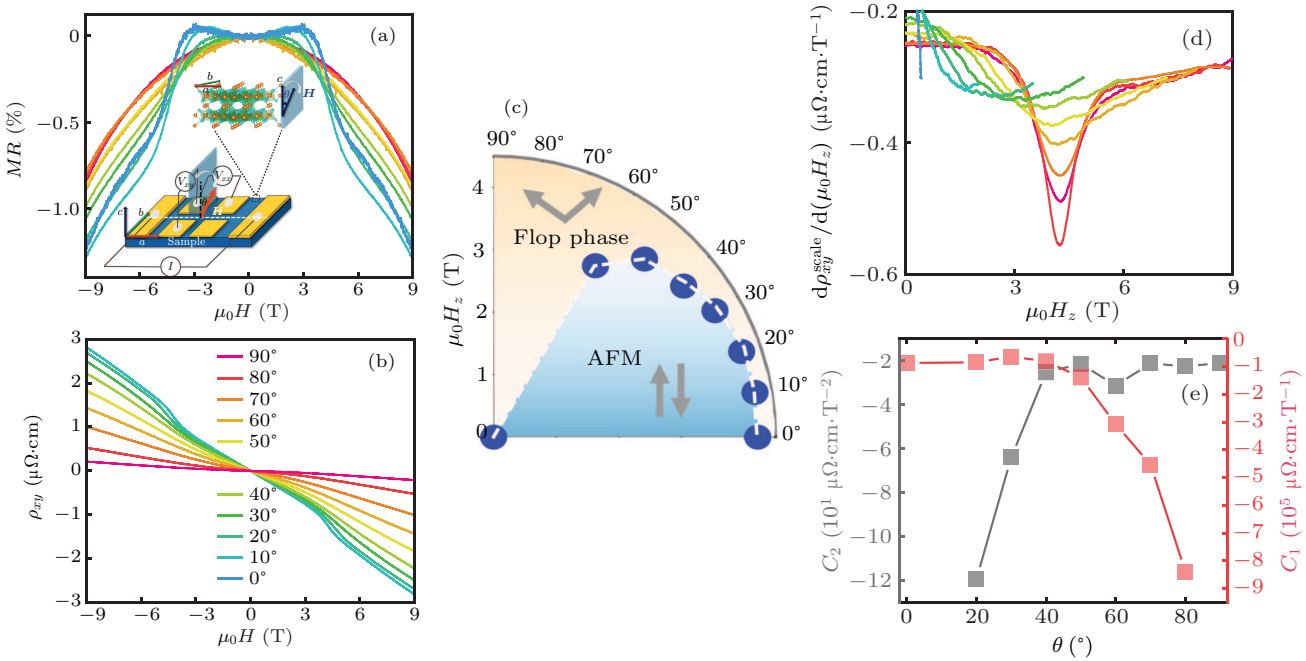


Fig. 3. Field dependent *MR* (%) (a) and Hall resistivity $\rho_{xy}(\theta)$ (b) at 2 K with $\theta = 0°$–$90°$ respectively. Inset of (a): The configuration of angular-dependent transport measurements for V_5S_8. The gray arrow indicates the rotating direction of the applied field. The current is along the *a* axis, and θ represents the angle between the applied field and *c* axis. (c) The phase diagrams in the polar coordinates with rotating applied field for V_5S_8. (d) $\mathrm{d}\rho_{xy}^{\mathrm{scale}}/\mathrm{d}\mu_0 H_z$ at different angles. (e) The angular dependence of C_1 and C_2 described by Eq. (2).

3.3. Planar Hall effect and anisotropic magnetoresistivity

PHE and PAMR are transport phenomena driven by an in-plane magnetic-field-induced rotation of the principal axes of the resistivity tensor.[41] As shown in the inset of Fig. 4(a), the applied field rotates within the *ab* plane of the crystal for the measurements. Obvious PHE and PAMR exhibit two-fold oscillatory angular dependence as shown in Figs. 4(a)–4(d). Usually the planar Hall and anisotropic mageto-resistivity can be described by

$$\begin{aligned} \rho_{xy}^{\mathrm{P}} &= -\Delta\rho \sin\phi\cos\phi, \\ \rho_{xx}^{\mathrm{P}} &= \rho_{\parallel}^{\mathrm{P}} + \Delta\rho \sin^2\phi, \end{aligned} \tag{3}$$

where ρ_{xy}^{P} represents the planar Hall resistivity. $\rho_{\parallel}^{\mathrm{P}}$ represents the magnetoresistivity parallel to the current. $\Delta\rho = \rho_{\perp}^{\mathrm{P}} - \rho_{\parallel}^{\mathrm{P}}$, where $\rho_{\perp}^{\mathrm{P}}$ represents the magnetoresistivity perpendicular to the current. And ϕ represents the angle between the applied field and current.[41] Recently, the research reveals the nontrivial topological nature for PHE and PAMR in topological materials which makes these phenomena useful ways to probe the interplay of spin, lattice and electron in nontrivial topological system. For an example, in Weyl semimetals with edge states, chiral anomaly and nontrivial Berry curvature effects engender transverse Hall voltage within the plane for the applied current and magnetic field precisely in a configuration in which the conventional Hall effect vanishes.[42] To investigate the origin of PHE and possible nontrivial topological electron structure for V_5S_8, the parametric plots of $\rho_{xy}^{\mathrm{P}}(\phi)$ and $\Delta\rho_{xx}^{\mathrm{P}}(\phi)$ are presented in Fig. 4(d). For Weyl semimetals, in the chiral anomaly regime, $\Delta\rho_{xx}^{\mathrm{P}}$ decreases intrinsically with increasing $\mu_0 H$, while $\rho_{xy}^{\mathrm{P}}(\pi/2)$ increases by roughly the same fraction. The balanced changes lead to closed contours that expand roughly isotropically from the zero-$\mu_0 H$ point. Moreover, the contour calipers $\Delta\rho_{xx}^{\mathrm{P}}$ approach saturation at large $\mu_0 H$s. In contrast, the case is quite different for V_5S_8. In weak $\mu_0 H$, the contours show small loops circling the zero-$\mu_0 H$ point. As $\mu_0 H$ increases, they expand dramatically away from the zero-$\mu_0 H$ point in the direction of increasing $\Delta\rho_{xx}^{\mathrm{P}}$, exhibiting a shock wave shape. These behaviors indicate that the anisotropic orbital *MR* or the spin-dependent scattering leads to prominent PHE in V_5S_8 instead of the origin of topological chiral anomaly.

We further check the field and temperature dependent $\Delta\rho_{xx}^{\mathrm{P}}$ shown in Figs. 4(f) and 4(g), respectively. In V_5S_8, the $\Delta\rho_{xx}^{\mathrm{P}}$ monotonous increases with increasing the applied field or decreasing the temperature. If the anisotropic ordinary magnetoresistivity dominates the PHE, the amplitude $\Delta\rho_{xx}^{\mathrm{P}}$ should be proportional to the square of the applied field. Here, we fit the data by using quadratic and linear functions respectively. It is found that the later fitting will give better results, suggesting the linear $\mu_0 H$ dependence of $\Delta\rho_{xx}^{\mathrm{P}}$ for V_5S_8. For PHE from the conventional origin in an isotropic magnetic system, they can be expressed as

$$\rho_{xy}^{\mathrm{P}} = \beta M_{\parallel}^2 \sin\phi\cos\phi, \tag{4}$$

where $M_{\parallel}$ is the in-plane magnetization and β is a constant. According to this formula, the amplitude $\Delta\rho_{xx}^{\mathrm{P}}$ should be proportional to the in-plane $M_{\parallel}^2$. Though V_5S_8 is an AF metal, the magnetization from canted AF moments by applied field

induces prominent PHE especially for that in the high field region. With increasing the temperature, the decrease of $\Delta\rho_{xx}^{\mathrm{P}}$ is consistent with the rapid shrinking magnetization. Recently, the high-order oscillatory components of PHE and PAMR were observed in KV_3Sb_5[43] and Sr_2IrO_4 films,[44] which suggests more complicated interaction such as magnetocrystalline anisotropy and spin–orbital coupling. For V_5S_8 in all temperature regions, PHE and PAMR keep two-fold angular oscillations, indicating the origin from the spin-dependent scattering in the magnetic system.[43]

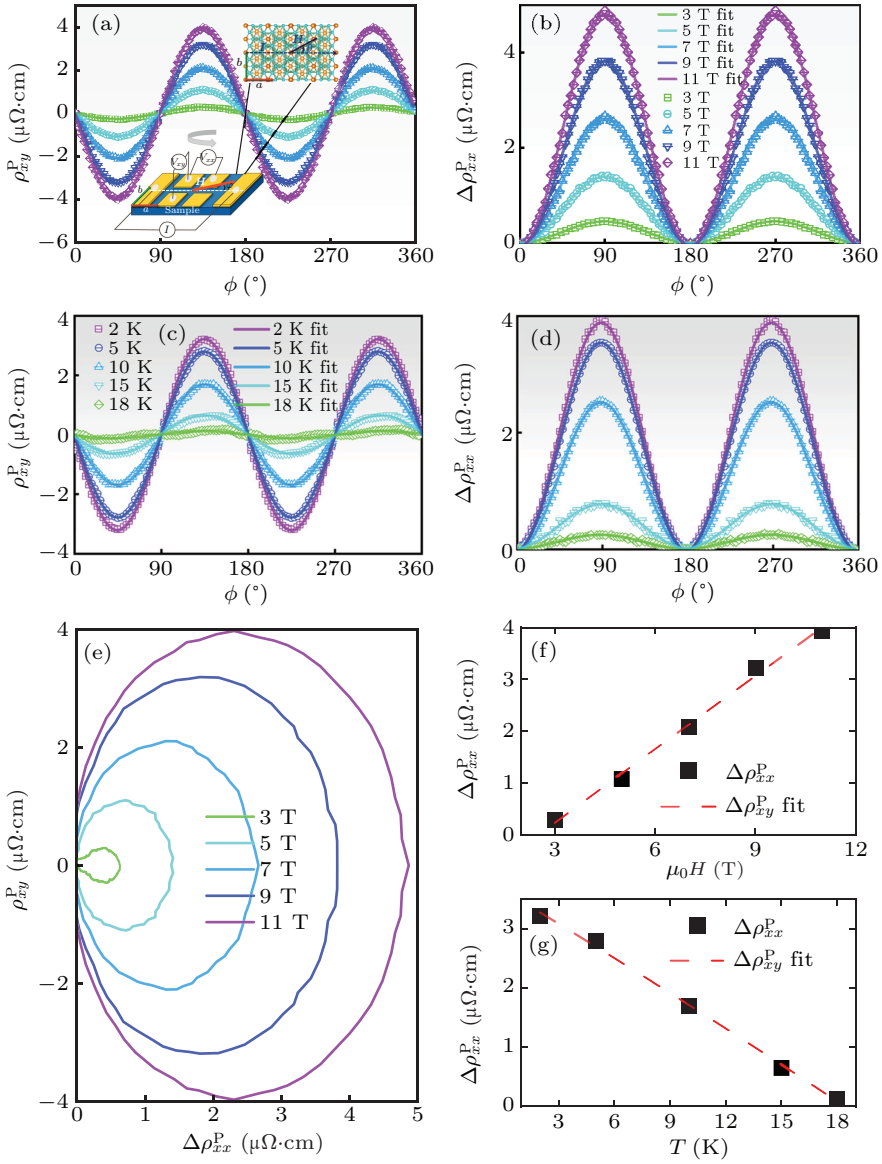


Fig. 4. Planar Hall resistivity $\rho_{xy}^{\mathrm{P}}(\phi)$ (a) and anisotopic magnetoresistivity $\Delta\rho_{xx}^{\mathrm{P}}(\phi)$ (b) at 2 K with $\mu_0 H = 3$ T, 5 T, 7 T, 9 T, 11 T, respectively. Inset of (a): The configuration of planar transport measurements for V_5S_8. The gray circular arrow indicates the rotating direction of the applied field. The current is along the a axis, and ϕ represents the angle between the applied field and current. The scatters represent the experimental data, while the curves represent the fitting results. Temperature dependent $\rho_{xy}^{\mathrm{P}}(\phi)$ (c) and $\Delta\rho_{xx}^{\mathrm{P}}(\phi)$ (d) with $\mu_0 H = 9$ T at 2 K, 5 K, 10 K, 15 K, 18 K, respectively. (e) The parametric plots obtained by plotting $\Delta\rho_{xx}^{\mathrm{P}}(\phi)$ and $\rho_{xy}^{\mathrm{P}}(\phi)$ with angle ϕ as the data for the x-axis and the data for the y-axis. The amplitude of planar resistivity at different magnetic field (f) and different temperature (g).

4. Conclusion

The angular and planar transport properties are systemically investigated for AF V_5S_8. Obvious AHE is observed in a flopped AF state with the Hall angle comparable to those in FM system. The SR magnetism makes AHE persist above the AF transition. The phase diagram by rotating the applied field reveals a spin-flop line with anisotropic Hall effect and *MR* for different magnetic states, which can be attributed to the magnetocrystalline anisotropy and anisotropic orbital scattering. Prominent PHE and PAMR in V_5S_8 exhibit two-fold angular oscillations systematically evolving with the temperature and the applied field, which is attributed to origin from the spin-dependent scattering. Our observations facilitate a deeper understanding of the interactions of magnetism and electron in V_5S_8 and provide information for potential AF spintronic application as the magnetic sensors and nonvolatile memory devices.

Acknowledgements

Project supported by the open research fund of Songshan Lake Materials Laboratory (Grant No. 2021SLABFN11), the National Natural Science Foundation of China (Grant Nos. U2130101 and 92165204), Natural Science Foundation of Guangdong Province (Grant No. 2022A1515010035), Guangzhou Basic and Applied Basic Research Foundation (Grant No. 202201011798), the Open Project of Guangdong Provincial Key Laboratory of Magnetoelectric Physics and Devices (Grant No. 2022B1212010008), the Open Project of Key Laboratory of Optoelectronic Materials and Technologies (Grant No. OEMT-2023-ZTS-01), the National Key R&D Program of China (Grant Nos. 2023YFF0718400 and 2023YFA1406500), and (national) college students innovation and entrepreneurship training program, Sun Yat-sen University (Grant No. 202310359).

References

[1] Elphick K, Frost W, Samiepour M, Kubota T, Takanashi K, Sukegawa K, Mitani S and Hirohat A 2021 *Sci. Technol. Adv. Mater.* **22** 235
[2] Smejkal L, Mokrousov Y, Yan B H and MacDonald A H 2018 *Nat. Phys.* **14** 242
[3] Ghimire N J, Botana A, Jiang J S, ZhangJ J, Chen J S and Mitchell J F 2018 *Nat. Commun.* **9** 3280
[4] Shekhar C, Kumar N, Grinenko V, *et al*. 2018 *Proc. Natl. Acad. Sci. USA* **115** 9140
[5] Kimata M, Chen H, Kondou K, Sugimoto S, Muduli P K, Ikhlas M, Omori Y, Tomita T, MacDonald A H, Nakatsuji S and Otani Y 2019 *Nature* **565** 627
[6] Zhang W F, Han W, Yang S H, Sun Y, Zhang Y, Yan B and Parkin S S 2016 *Sci. Adv.* **2** e1600759
[7] Smejkal L, Sinova J and Jungwirth T 2022 *Phys. Rev. X* **12** 040501
[8] Duan X D, Wang C, Pan A L, Yu R Q and Duan X F 2015 *Chem. Soc. Rev.* **44** 8859
[9] Choi W, Choudhary N, Han G H, Park J, Akinwande D and Lee Y H 2017 *Mater. Today* **20** 116
[10] Deng Y, Yu Y, Shi M Z, Guo Z X, Xu Z H, Wang J, Chen X H , and Zhang Y B 2016 *Science* **367** 895
[11] Wang Y, Sofer Z, Luxa J and Pumera M 2016 *Adv. Mater. Interfaces* **3** 1600433
[12] Sugawara K, Nakata Y, Fujii K, Nakayama K, Souma S, Takahashi T and Sato T 2019 *Phys. Rev. B* **99** 241404
[13] Guo Y Q, Deng H T, Sun X, *et al*. 2017 *Adv. Mater.* **29** 1700715
[14] Schrieffer J R and Wolff P A 2016 *Phys. Rev.* **149** 491
[15] Schrieffer J 1967 *J. Appl. Phys.* **38** 1143
[16] Coqblin B and Schrieffer J 1969 *Phys. Rev.* **185** 847
[17] Endo M, Kanai S, Ikeda S, Matsukura F and Ohno H 2010 *Appl. Phys. Lett.* **96** 21
[18] Hardy W J, Yuan J T, Guo H, Zhou P P, Lou J and Natelson D 2016 *ACS Nano* **10** 5941
[19] Niu J J, Yan B M, Ji Q Q, Liu Z F, Li M Q, Gao P, Zhang Y F, Yu D P and Wu X S 2017 *Phys. Rev. B* **96** 075402
[20] Zhang R Z, Zhang Y Y and Du S X 2020 *Chin. Phys. B* **29** 077504
[21] Zhou Z, Zhao X X, Wu L M, *et al*. 2022 *Phys. Rev. B* **105** 235433
[22] Yan C J, Chen L N, Zhou K Y, Yang L P, Fu Q W, Wang W Q, Yue W C, Liang L K, Tao Z and Du J 2023 *Chin. Phys. B* **32** 017503
[23] Kim Y S, Brahlek M, Bansal N, Edrey E, Kapilevich G A, Iida K, Tanimura M, Horibe Y, Cheong S W and Seongshik O 2011 *Phys. Rev. B* **2** 073109
[24] Lupke F, Pham A D, Zhao Y F, Zhou L J, Lu W C, Briggs E, Bernholc J, Kolmer M, Teeter J, Kolmer M, Teeter J, Ko W, Chang C Z, Ganesh P and Li A P 2022 *Phys. Rev. B* **105** 035423
[25] Zhou J D, Zhang W J, Lin Y C, *et al*. 2022 *Nature* **609** 46
[26] Silbernagel B G, Levy R and Gamble F R 1975 *Phys. Rev. B* **11** 4563
[27] Nozaki H, Umehara M, Ishizawa Y, Saeki M, Mizoguchi T and Nakahira M 1978 *JPCS* **39** 851
[28] Nakanishi M, Yoshimura K, Kosuge K, Goto T, Fujii T and Takada J 2000 *J. Magn. Magn. Mater.* **221** 301
[29] Balents L 2010 *Nature* **464** 199
[30] Nagaosa N, Sinova J, Onoda S, MacDonald A H and Ong N P 2010 *Rev. Mod. Phys.* **82** 1539
[31] Markou A, Taylor J, Kalache A, Werner P, Parkin S and Felser C 2010 *Phys. Rev. Mater.* **2** 051001
[32] Manna K, Muechler L, Kao T H, *et al*. 2018 *Phys. Rev. X* **8** 041045
[33] Zhang Y, Deng K, Zhang X, Wang M, Wang Y, Liu C, Mei J W, Kumar S, Schwier E F, Shimada K, Chen C Y and Shen B 2020 *Phys. Rev. B* **101** 205126
[34] Yi E K, Zheng D F, Pan F H, Zhang H X, Wang B, Chen B W, Wu D T, Liang H L, Mei Z X, Wu H, Yang S Y, Cheng P, Wang M and Shen B 2023 *Phys. Rev. B* **107** 035142
[35] Xu Y, Das L, Ma J Z, Yi C J, Nie S M, Shi Y G, Tiwari A, Tsirkin S S, Neupert T, Medarde M, Shi M, Chang J and Shang T 2021 *Phys. Rev. Lett.* **126** 076602
[36] Funahashi S, Nozaki H and Kawada H 1981 *J. Phys. Chem. Solids* **42** 1009
[37] Zhao J J, Jiang B Y, Zhang S, Wang L J Y, Liu E, Li Z L and Wu X S 2023 *Phys. Rev. B* **107** 085203
[38] Fleury P A 1969 *Phys. Rev.* **180** 591
[39] Schindler A I and LaRoy B C 1971 *Solid State Commun.* **9** 1817
[40] Fujishiro Y, Kanazawa N, Kurihara R, Ishizuka H, Hori T, Yasin F S, Yu X, Tsukazaki A, Ichikawa M, Kawasaki M, Nagaosa N, Tokunaga M and Tokura Y 2021 *Nat. Commun.* **12** 317
[41] Koch K 2016 *Z. Naturforsch. A* **10** 496
[42] Nandy S, Sharma G, Taraphder A and Tewari S 2017 *Phys. Rev. Lett.* **119** 176804
[43] Li L Y, Yi E K, Wang B, Yu G Q, Shen B, Yan Z B and Wang M 2023 *npj Quantum Mater.* **8** 2
[44] Liu M R, Yue J N, Meng J C, Shao T N, Yao C L, Sun X J, Nie J C and Li D B 2023 *Appl. Phys. Lett.* **122** 022402